Fractal properties from 2D-curvature on multiple scales

Erhardt Barth[#], Christoph Zetzsche[&], Mario Ferraro*, and Ingo Rentschler[#]

[#]Institut für Medizinische Psychologie, Goethestr. 31, 8000 München 2, Germany.

[&]Lehrstuhl für Nachrichtentechnik, Technische Universität München, Arcisstr. 21, 8000 München 2, Germany.

[*]Dipartimento di Fisica Sperimentale, via Giuria 1, 10125 Torino, Italy.

ABSTRACT

Basic properties of 2D-nonlinear scale-space representations of images are considered. First, local-energy filters are used to estimate the Hausdorff dimension, D_H, of images. A new fractal dimension, D_N, defined as a property of 2D-curvature representations on multiple scales, is introduced as a natural extension of traditional fractal dimensions, and it is shown that the two types of fractal dimensions can give a less ambiguous description of fractal image structure. Since fractal analysis is just one (limited) aspect of scale-space analysis, some more general properties of curvature representations on multiple scales are considered. Simulations are used to analyse the stability of curvature maxima across scale and to illustrate that spurious resolution can be avoided by extracting 2D-curvature features.

1. INTRODUCTION

Many processes shaping our physical environment produce fractal surfaces, i.e, surfaces characterized by a fractal dimension [8][12]. Furthermore, it has been shown that isotropic Lambertian fractal surfaces of constant albedo yield fractal images [13]. Thus, one should expect the fractal dimension to reflect statistical properties of natural images. The fractal dimension of surfaces and curves has been related to human perception, e.g., the perception of roughness [13] and the ability of humans to perceive shapes when looking at patterns with fractal contours [15].

In the natural sciences, the theory of fractal sets is relevant to investigations of changes of a physical quantity when the degree of coarse-graining in observation (scale) is changed. Similar problems arise in computer vision, in the sense that visual systems (artificial or biological) must operate on multiple scales, and indeed there is evidence that the visual input is processed by different types of neurons at multiple levels of resolution[16]. In this paper we investigate how different models of visual neurons can be related to fractal analysis, in the sense that the difference of activity of self-similar filters is related to the fractal dimension of the image. It will be shown, however, that the computation of only one fractal dimension is not sufficient for capturing fractal properties of images. This is because a "line" (an object with topological dimension $d_T = 1$) with a certain fractal dimension will look like a coastline, but a fractal "surface" will not necessarily look like a natural landscape. Also, two surfaces with the same fractal dimension can *look* very different (see Figure 1). We will point out that this problem can be solved by introducing a new fractal dimension, D_N, defined as a property of 2D-curvature scale space[a].

The possibility to generate fractal landscapes and other patterns which look natural (and nice) was a major argument for the application of fractal ideas. In [4] simple algorithms operating with curvature at different levels of resolution were used to generate such fractal landscapes and patterns.

---

a. Introducing a new fractal dimension is in accordance with the current state of affairs in the fractal sciences which are "far from a complete understanding of fractal dimensions" [17].

87 SPIE Vol. 2031, *Geometric Methods in Computer Vision*, B. Vemuri, editor, 87-99, 1993.

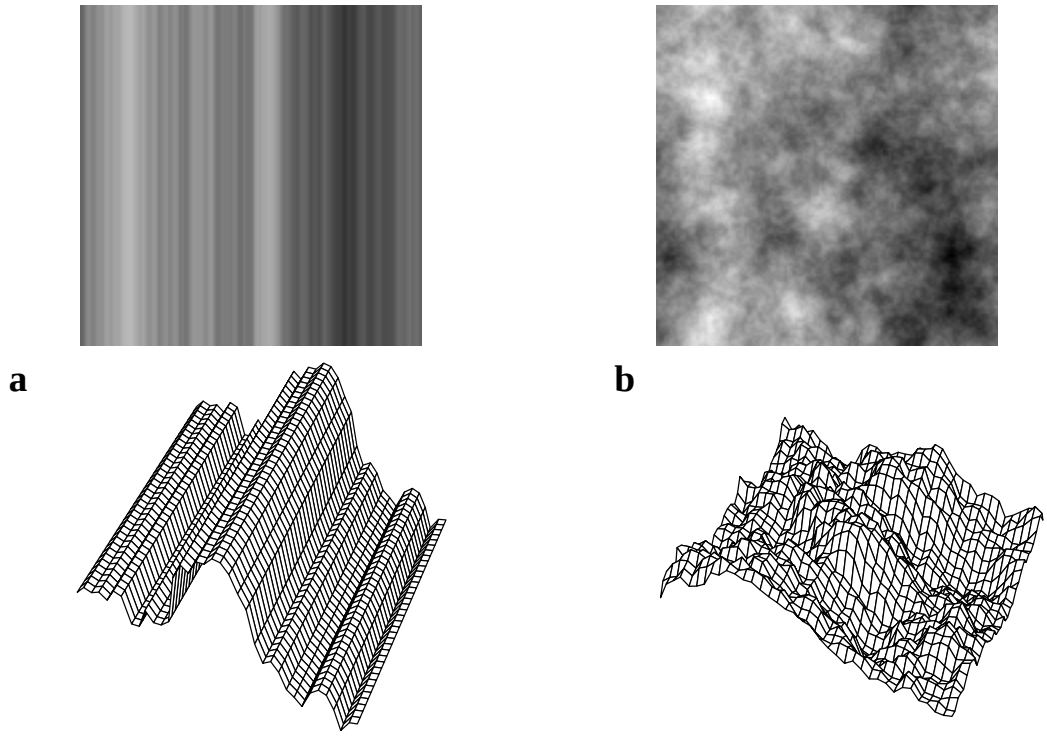

Figure 1. Two self-similar fractal images (top) with the same fractal dimension $D = 2.5$ and the corresponding partial surface plots (below). The fractal cylinder in **a** *has been obtained by extending a cut through the image* **b** *to full height It should be clear that if a traditional fractal measure "reports" to see a fractal landscape with $D = 2.5$ we can not know whether it looks like in* **a** *or like in* **b**. *We might, of course, find practical algorithms giving different results for* **a** *and* **b**, *but the theoretical measures these algorithms are supposed to approximate (e.g., the Hausdorff- or capacity dimensions) are the same.*

Although the fractal dimension is the most basic quantity for the representation of self similar shapes, it is impossible to describe more complex shapes with only one number [17][a]. These limitations lead us to study more general scale-space properties. In computer vision it is well accepted that the visual system uses representations on multiple scales, and different approaches based on the idea of a *linear* scale space have been presented. However, any vision system needs to represent shape, and most image (or object) properties related to shape involve non-linear operations. Indeed, nonlinear 2D-detectors have been found in the visual cortex (hypercomplex- and dot-responsive cells). These neurons are sensitive to intrinsically two-dimensional features like line ends or corners. They ignore 1D-signals (parabolic surface regions in the sense of differential geometry) like straight lines or straight edges. Possible relationships between curvature and the end-stopping property of these neurons have been pointed out by several authors (see [20] for a discussion). Models for these neurons have been derived from filter theory and differential geometry [21][20]. They are based on the concept of intrinsic dimensionality and have been related to image coding. In particular, it has been shown that images can be reconstructed from a 2D-curvature scale-space representation [2][24][3]. Linear scale space and nonlinear shape features are usually linked by assuming that the nonlinear features are extracted from the linear scale space at several scales. We suggest that these nonlinear multi-scale features should be studied in the framework of a non-linear scale space which will have a structure different from the original (linear) one. As to our knowledge, a general treatment of

a. Extensions of fractal dimensions and multi-fractals are current topics of fractal theory.

nonlinear scale space has not been published as yet, and the problem will not be solved in this paper. However, we will show that a 2D-curvature scale-space based on the above mentioned concepts has several advantages over a linear scale space.

2. FRACTAL PROPERTIES

2.1 Measuring fractal dimensions

"Fractal dimension" is a generic name for dimensions which can take fractional values [17] (see Table 1).

Table 1. Definitions for different dimensions - adapted from [17].

Symbol	Name	Definition
d	Euclidean dimension	Dimension of the Euclidean space in which the observed set is embedded. Takes integer values only.
d_T	Topological dimension	Takes integer values only. Defined as the dimension of the geometric object on which a set can be transformed by a continuous mapping (0 for a point, 1 for a line,...).
D	Fractal dimension	Generic terminology without strict definition; often identified with Hausdorff dimension or capacity dimension.
D_S	Similarity dimension	Defined for strictly self-similar objects.
D_H	Hausdorff dimension	Defined by most efficient covering.
D_C	Capacity dimension	Defined by covering with identical spheres or cubes.
D_I	Information dimension	Calculated from a probability distribution.
D_L	Lyapunov dimension	Used to characterise the dimension of the chaotic attractor.
D_F	Fourier dimension	Defined by the decrease of the power spectrum.

Formally, a fractal surface is a set belonging to $\Re^3$, such that its Hausdorff dimension, D_H, is fractional, and $2 \le D_H \le 3$. Usually it is assumed that fractal surfaces are self-affine and isotropic but in general this is not always the case [17][8][12].

It has been claimed that "dimension provides the natural vehicle to make the notion of degree of freedom more precise"[5]. This statement can be made more clear if one considers the difference between the Euclidean dimension and the topological dimension. The Euclidean dimension, i.e., the dimension of the space in which the set is embedded, gives the maximum number of possible degrees of freedom for every point of a set, whereas the topological dimension defines the degree of freedom remaining when the constraints that specify the membership to the set are enforced. Thus, each element of a set of points in a 3D space has 3 degrees of freedom, but if this set is supposed to form a surface all points must satisfy the constraint $F(x, y, z) = 0$ for some function F. The degrees of freedom reduce to 2, that this the topological dimension of a surface. This relation can be extended to the case of fractional dimensions if one considers the notion of information dimension [5]. This dimension measures the quantity of information about the state of a system gained when making a measurement. It can be proved that the similarity dimension, and, in most cases of interest, the Hausdorff dimension are an upper bound for the information dimension, obtained when the asymptotic distribution is supposed to be uniform.

From an image processing point of view, it is possible to introduce a different definition of dimension, the *intrinsic* dimension, which is connected with the redundancy of a two-dimensional signal and the surface types in differential geometry [2][24][3]. Roughly speaking, redundancy occurs if a process does not use its degrees of freedom. Thus planar surfaces (0D-image regions) have intrinsic dimension 0 - they do not use any degree of

freedom. Parabolic surfaces correspond to 1D-regions since they use only one degree of freedom. Only surfaces with Gaussian curvature different from zero (2D regions) have no clear (integer) restriction of their dimensionality. In analogy, we look for intrinsic fractal dimensions which are closer to a global quantification of how far a system *uses* it's degrees of freedom.

From a signal processing point of view, the fractal dimension D can be derived from a power spectrum of the form $S(\rho, \theta) = \rho^{-\beta_2}$ with $2 < \beta_2 < 4$. The fact that the power spectra of most natural images lie within this range is well known[a] and has been used in standard image coding. Modern coding techniques, however, have to make use of more complex (higher order) statistical dependencies in natural images[24].

2.1.1 Isotropic fractals

Let $\{G_i\}$ be a family of band-pass filters, defined, in polar coordinates ρ, θ, as

$$G_i(\rho, \theta) = M\left(\log\frac{\rho}{\rho_i}\right)\phi(\theta), \tag{1}$$

and let the domain of definition of the filter be the interval $[\rho_i/a, a\rho_i]$, where a is a constant. Further suppose that any filter is the copy of any other, translated along a logarithmic scale $\log(\rho)$, and that their centres are equally spaced along this scale.

Let $S(\rho, \theta) = \rho^{-\beta_2}$ be an isotropic two-dimensional power spectrum. Define

$$R_i = \int\int \rho^{-\beta_2} G_i^2(\rho, \theta)\, \rho\, d\rho\, d\theta = \int_{\rho_i/a}^{a\rho_i} \rho^{-\beta_2+1} M^2(\log(\rho/\rho_i))\, d\rho \int_0^{2\pi} \phi^2(\theta)\, d\theta. \tag{2}$$

Set $c_1 = \int_0^{2\pi} \phi^2(\theta)\, d\theta$ and $y = \rho/\rho_i$, then

$$R_i = c_1 \rho_i^{-\beta_2+2} \int_{1/a}^{a} y^{-\beta_2+1} M^2(\log(y))\, dy. \tag{3}$$

A straightforward application of the mean-value theorem [6] shows that

$$R_i = c_1 \xi_i^{-\beta_2+2} \int_{1/a}^{a} y^{-1} M^2(\log(y))\, dy, \tag{4}$$

where ξ_i belongs to the interval $[\rho_i/a, a\rho_i]$. Then

$$R_i = c_1 \xi_i^{-\beta_2+2} \int_{-\log a}^{\log a} M^2(z)\, dz, \tag{5}$$

where $z = \log y$.

The result of the integral in Eq. 5, say c_2, is the same for every filter, and finally we can write

$$R_i = c_1 c_2 \xi_i^{-\beta_2+2} = c\xi_i^{-\beta_2+2} \tag{6}$$

---

a. This is the main reason why Fourier methods have been used with success in electrical engineering, allowing to separate the signal from the noise.

When plotted on a log-log scale, the responses are distributed along a straight line whose slope is $2 - \beta_2$. Then

$$2 - \beta_2 = \frac{\log R_{i+1} - \log R_i}{\log \xi_{i+1} - \log \xi_i} \tag{7}$$

It has been proved [18] that for a two-dimensional, isotropic random process with a power spectrum $S(\rho, \theta) = \rho^{-\beta_2}$, the Hausdorff dimension is given by

$$D_H = 3 - \left(\frac{\beta_2 - 2}{2} \right) \tag{8}$$

Define

$$\frac{\log R_{i+1} - \log R_i}{2 (\log \xi_{i+1} - \log \xi_i)} = -F_R, \tag{9}$$

then Eq. 8 becomes

$$D_H = 3 - F_R. \tag{10}$$

2.1.2 Fractal cylinders

It has been shown that the Hausdorff dimension of a curve γ can be computed by considering the spectral density $S(f)$ of γ, and in particular it has been proved [18] that if $S(f) \sim f^{-\beta_1}$, the Hausdorff dimension is given by

$$D_H = \frac{5 - \beta_1}{2}. \tag{11}$$

The calculation of the Hausdorff dimension of surfaces can be reduced to the computation of the dimension of curves γ obtained by intersecting the surface with a plane. The basis for this method is provided by a theorem due to Mattila [10], which generalized a previous result by Marstrand [9].

Let S be a set in $\Re_n$ with Hausdorff dimension $D_H(S) = s$; then, if $s > n - m$ for almost all m planes V through almost all points in $S \cap V$,

$$D_H(S \cap V) = s + m - n. \tag{12}$$

Then in case of $n = 3$ and $m = 1$, it follows that the intersection of a plane with a surface S with Hausdorff dimension s gives rise to a curve of Hausdorff dimension $s - 1$ for almost all planes V through almost all points of S.

Thus if a cut γ of the surface S has dimension $D_H(\gamma) = s - 1$, then $D_H(S) = s$ and it is obvious that

$$D_H(S) = \frac{7 - \beta_1}{2}. \tag{13}$$

Note that this result does not depend on the assumption of isotropy. In the isotropic case $\beta_1 = \beta_2 - 1$ in accordance with Eq. 8.

Consider a geometrical object with $d_T = 1$ and $D = 1.5$ (a fractal curve) generated by, e.g., one-dimensional Brownian motion. We now build up a surface ($d_T = 2$) as a Cartesian product of the original set with a line (a fractal cylinder) - see Figure 1. Since the power spectrum of a fractal cylinder is restricted to a line, we have $\beta_2 = \beta_1$.

It is straightforward to show, with calculations similar to those in the previous section, that in this case the relationship between β_2 and R_i is given by

 SPIE Vol. 2031, *Geometric Methods in Computer Vision*, B. Vemuri, editor, 87-99, 1993.

$$1 - \beta_2 = \frac{\log R_{i+1} - \log R_i}{\log \xi_{i+1} - \log \xi_i} \tag{14}$$

Inserting Eq. 7 in Eq. 13, we obtain an expression for the fractal dimension identical to the one given by Eq. 10. It must be stressed that Eq. 10 holds for both, isotropic fractals and fractal cylinders. (In general the relation between β_1 and β_2 is more complicated and the result of the estimation will depend on the angular tuning of the filters. The results presented in Figure 3 suggest that Eq. 10 can bee used with good approximation.)

2.2 Fractal dimension based on 1D local-energy filters

In order to estimate the power spectra with measures localized in frequency and space, it is reasonable to use even and odd filter pairs and to compute their local energy (this operation can be used as a model for complex cells [1][25][11][19] - see also Appendix).

From Eq. 12 it follows that almost all cuts through the surface will have the same fractal dimension. Thus, traditional fractal measures perform an "OR-like" (arithmetic mean) combination of orientations in multi-dimensions. We therefore use an operator $L_i(x, y)$ defined as the sum of local-energy filter outputs (complex cell model) at different orientations to compute a fractal dimension in the following way:

$$D_L = 3 - F_L, \tag{15}$$

where F_L is defined in Eq. 10 with $R = L$ (for the definition of L see Appendix).

D_L gives very good estimates of the Hausdorff dimension as illustrated in Figure 2. For the images in Figure 1, we get $D_L = 2.56$ for **a** and $D_L = 2.48$ for **b**.

In the actual computations the difference $\log \xi_{i+1} - \log \xi_i$ in Eq. 10 has been approximated by $\log \rho_{i+1} - \log \rho_i$, and the values F_R obtained from two successive scales where averaged across four scales for 128*128 images. Small constants have been added to L such that $D_{L,N} = 0$ in the degenerate case of zero activity in all filters.

2.3 Intrinsic fractal dimension based on 2D local-energy

The natural alternative to the "OR-like" processing of different orientations is "AND-like" combination. We have shown that the computation of curvature is, in essence, a specific type of "AND-processing" across orientation governed by the compensation principle [20][21]. With a procedure analogous to that used for D_L, we define a curvature based dimension D_N as (for the definition of the operator N see Appendix)

$$D_N = 3 - F_N. \tag{16}$$

The measure D_N can be seen as a synthesis of concepts related to curvature, intrinsic dimensionality and fractal dimensions. Gaussian curvature can only be defined for smooth surfaces. Using the concept of intrinsic dimensionality and the compensation principle one can define intrinsic-2D measures, in analogy to Gaussian curvature, on a more general filter basis. These measures can then be used to define an intrinsic dimension like D_N. Our preference for the operator N is due to the fact that it computes a 2D-local *energy*. The filter size and spacing has been adapted to assumptions about the properties of visual neurons. The measure D_N, however, can be seen more generally as not depending on a specific implementation of N. The basic requirements for N are that it should be a 2D-curvature operator (and thus not respond to parabolic regions), and that it can estimate the spectral density as tested in Figure 2. For isotropic fractals, D_N gives very good estimates of the Hausdorff dimension. For the images in Figure 1, we get $D_N = 2.51$ for **a** and $D_N = 0$ for **b**. It must be observed that, for D_N, the fractal cylinder is a degenerate case corresponding to zero activity in all filters. The value zero is somewhat arbitrary in that it depends on the normalization convention, but it is consistent with the fact that D_N is related to the curvature of the surface.

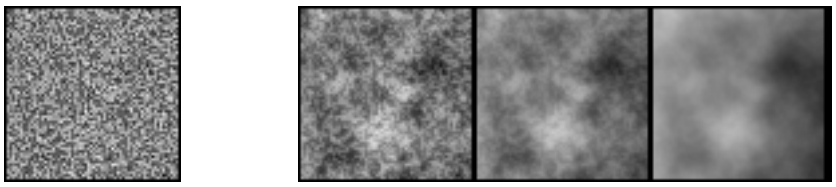

D_H	3	2.5	2
D_L	2.98	2.48	1.98
D_N	3.01	2.51	2.02

Figure 2. Test image for fractal dimension estimates. The image on the left (Gaussian white noise) was filtered such that the power spectra of the next images are given as $S(\rho, \theta) = \rho^{-\beta_2}$ *with* $\beta_2 = 2, 3, 4$ *from left to right. The values of the fractal dimensions are given below the corresponding images.*

Figure 3 illustrates how the two measures D_L and D_N can be used to span a two-dimensional fractal-feature space. Using only the traditional fractal dimensions a variety of fractal patterns between isotropic fractals and fractal cylinders are collapsed to a line (the 3 examples in Figure 3 have the same Hausdorff dimension).

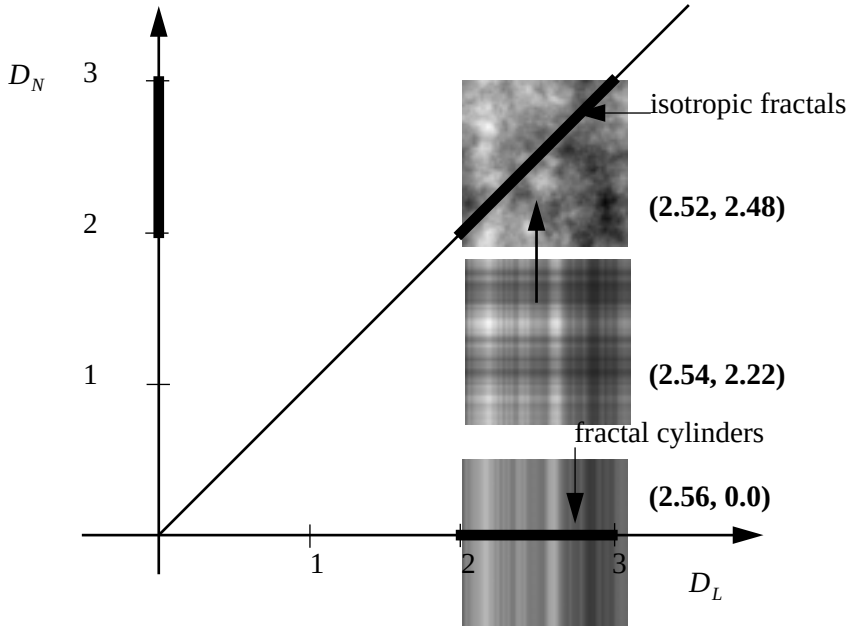

Figure 3. The two-dimensional fractal feature space. The pattern in the middle is the product of the fractal cylinder below ($D_H = 2.5$*) and a horizontal fractal cylinder with* $D_H = 2.25$*. The Hausdorff dimension, and thus* D_L*, is determined by the set with the highest dimension, whereas a measure like* D_N *is sensitive to the lowest fractal dimension. Thus, isotropic fractals will lie on the diagonal, fractal cylinders on the* D_L *axis, and all other fractals in between.*

 SPIE Vol. 2031, *Geometric Methods in Computer Vision*, B. Vemuri, editor, 87-99, 1993.

3. MORE GENERAL STRUCTURAL PROPERTIES OF A 2D-CURVATURE SCALE SPACE

In the previous section we argued that two dimensions are needed to capture the fractal structure of images. Here we just *point out* some further possibilities to derive image structure from nonlinear scale-space.

3.1 A differential result due to the diffusion equation

Let $l(x, y, s)$ denote the image intensity at different levels of resolution. Since the determinant of the Hessian defined as

$$det\,(H) \;=\; G \;=\; l_{xx}l_{yy} - l_{xy}^2 \tag{17}$$

can be seen as the 2D-curvature operator with the simplest analytical expression, we chose it to derive a simple nonlinear diffusion result by just looking at the derivative with respect to scale G_s:

$$G_s \;=\; l_{xx}l_{yys} + l_{xxs}l_{yy} - 2l_{xy}l_{xys} \quad . \tag{18}$$

Using the diffusion equation $l_s \;=\; \nabla^2 l$ which holds for Gaussian blurring, we obtain:

$$G_s \;=\; l_{xx}l_{yyyy} + l_{yy}l_{xxxx} + l_{xxyy}\,(l_{xx} + l_{yy}) \;-\; 2l_{xy}\,(l_{xxxy} + l_{yyyx}) \qquad . \tag{19}$$

Eq. 19 shows how changes with scale of a curvature operator can be expressed in terms of only spatial derivatives of $l(x, y, s)$. It also illustrates that G will change with scale only if the intensity l changes up to second *and* fourth order. To make this point more clear we consider only isotropic local maxima of l. For such points Eq. 19 simplifies to:

$$G_s \;=\; \frac{1}{2}\nabla^2 l \nabla^2\,(\nabla^2 l) \quad , \tag{20}$$

whereas a Laplacian scale-space would be governed by

$$(\nabla^2 l)_s \;=\; \nabla^2\,(\nabla^2 l) \quad .$$

(Note that Eq. 20 equally holds for the Gaussian curvature of a Monge patch defined by l.) However, by using the clipped-eigenvalues operator C (Eq. 29), we obtain a 2D-curvature scale-space with the equivalent of Eq. 20 as

$$C_s \;=\; \nabla^2\,(\nabla^2 l) \quad .$$

This is because C equals the Laplacian for zero eccentricity.

3.2 Stability of curvature maxima across scale

The figures in this section illustrate how the maxima, with respect to (x, y), of different representations change with scale. Simple geometric patterns are chosen to show the basic structure. A further example illustrates how the maxima corresponding to natural images fill in the scale-space. We expect such patterns to give a useful description of images in terms of local/global relationships in the curvature representations.

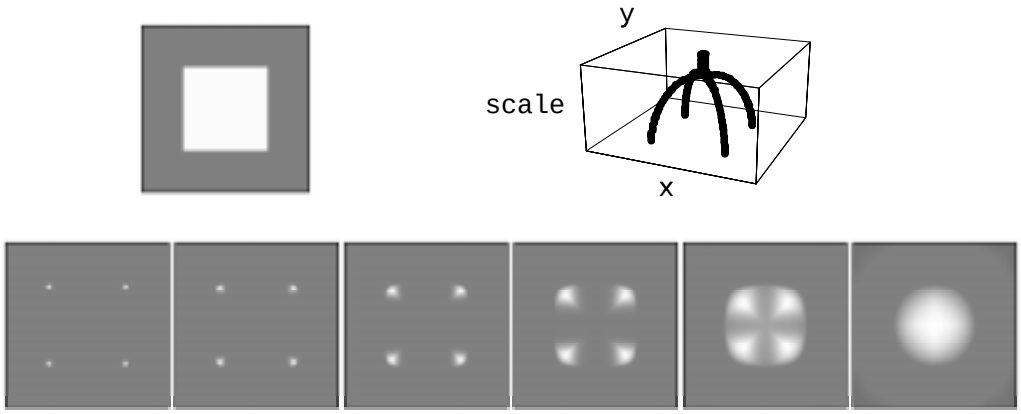

Figure 4. Maxima of curvature across scale. Input image (top left), six samples from the 2D scale-space based on the C operator (bottom), and position of maxima across scale (top right). For plotting the maxima, 64 scales have been computed by multiplying the cutoff frequency with a factor of 0.95 at each iteration. The positions of the maxima where obtained by thresholding the outputs at different scales with the same relative threshold of 0.5%.

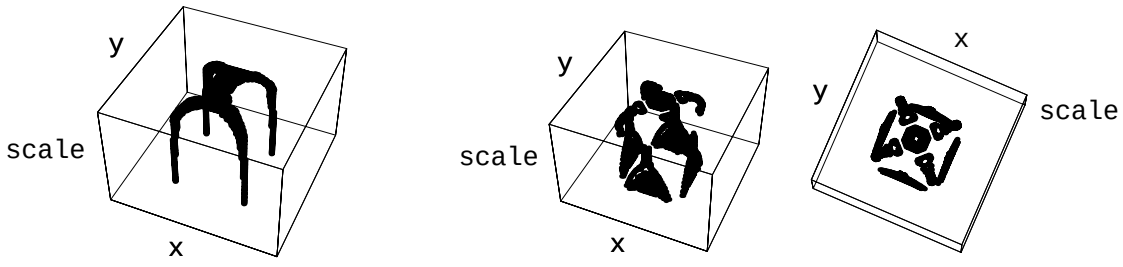

Figure 5. Maxima across scale for the local energy operators (same input as in Figure 4). The 2D local energy h (left - see Appendix Eq. 26) gives a consistent tree structure whereas for the 1D-local energy g (right - presented in two views) the maxima switch from the edges to the corners of the square.

 SPIE Vol. 2031, *Geometric Methods in Computer Vision*, B. Vemuri, editor, 87-99, 1993.

Figure 6. Examples of curvature maxima across scale illustrating feature merging (left - C operator) and a typical structure of the maxima corresponding to a natural image (right - the maxima of C^2 are plotted).

3.3 Avoiding spurious resolution.

The criterion of causality for a scale-space representation requires that no spurious details should be generated when the resolution is diminished [14] [7]. It has been shown that this condition implies that the normals of the isoluminance surfaces of the scale space must point towards lower scales [7]. A Laplacian scale-space obtained with Gaussian blurring will satisfy this condition under the assumption $G \neq 0$ for all (x, y) (Eq. 27). A scale-space based on the C operator is more consistent since the regions for which this condition does not hold (e.g., parabolic patches) are not represented.

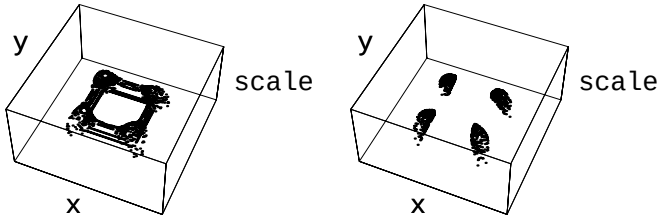

Figure 7. Isoluminance surfaces for Laplacian (left) and curvature operator C (dot-responsive cell model, right) for the same input as in Figure 4. The points in scale-space with values in a certain range where plotted as dots without interpolation. The Laplacian surface contains hyperbolic regions at the boundaries between corners and edges thus indicating the presence of spurious resolution - see text.

4. DISCUSSION

The fractal dimension, D_L, based on local-energy filter outputs (complex cell model) has been shown to be a very good approximation of the Hausdorff dimension, D_H. In addition, the curvature-based fractal dimension, D_N, has been introduced to obtain a better description of natural fractal shapes by resolving the ambiguity between fractal landscapes and fractal cylinders. We conclude that the visual system is well equipped for dealing with a fractal environment since both fractal dimensions can be computed from models for visual neurons (complex- and hypercomplex cells).

Our analysis of the "visual measurement of fractal properties" suggests that the latter should be treated as a specific aspect of the more general question of how intrinsically two-dimensional features vary across scale. We presented first steps towards such an analysis, showing that curvature maxima are stable across scales and that spurious resolution can be avoided. Thus, 2D-neurons, operating on multiple levels of resolution, can provide a consistent representation of the visual input.

5. ACKNOWLEDGEMENT

The work has been supported by the Deutsche Forschungsgemeinschaft grant Re 337/7 to I.R. and C.Z.

6. APPENDIX

The 1D- and 2D-local energy operators (complex- and hypercomplex cell models)

The operators are based on polar-separable band-pass filters defined as

$$G_j(\log\rho, \theta) = \left(\cos\frac{\pi}{2}\left(\frac{\log\rho - \log\rho_0}{\log\rho_b}\right)\right)^2 \left(\cos\frac{\pi}{2}\left(\frac{\theta - \theta_j}{\theta_b}\right)\right)^2 \tag{21}$$

with $\rho = \sqrt{u^2 + v^2}$ and $\theta = \text{atan}(u/v)$, with (u, v) being the coordinates of the Fourier transform, ρ_0 the central frequency, $\log\rho_b$ the radial bandwidth on a log scale, θ_j the orientation, and θ_b the angular bandwidth. The filters segment the (u, v) plane like pieces of a cake. The filters G_j at different orientations j have been used in even/odd pairs corresponding to the filter responses $g_{oj}(x, y)$ and $g_{ej}(x, y)$. The local energy response for one orientation j is defined as

$$a_j(x, y) = g_{oj}^2 + g_{ej}^2 \tag{22}$$

The quasi-isotropic operator used to estimate the fractal dimension D_L is defined as

$$L_i(x, y) = \iint g_i(x, y)dxdy, \tag{23}$$

where

$$g_i(x, y) = \sum_{j=1}^{n} a_j(x, y), \tag{24}$$

and $n = 8$ in our simulations. The integral of $g(x, y)$ with respect to (x, y) estimates the global energy, and thus the global fractal dimension of the image. Various degrees of low-passing of the activity $g(x, y)$ allows to treat the image as a multi-fractal with a fractal dimension associated to a certain image region.

The 2D local-energy operator is defined as

$$N_i(x, y) = \iint h_i(x, y)dxdy \tag{25}$$

where

$$\imath_i(x, y) = \sum_{j=1}^{n} \sqrt{a_j(x, y)a_{j+1}(x, y) - b_j^2(x, y)} \text{ with } a_{n+1} = a_1. \quad (26)$$

The compensation terms, $b_i(x, y)$, are defined in the same way as $a_i(x, y)$ (Eq. 22) but with an angular function $\frac{1}{2}\cos\pi\left(\frac{\theta - \theta_j}{\theta_b}\right)$ for the underlying filters. The orientation of the $b_i(x, y)$ lies in-between $a_i(x, y)$ and $a_{i+1}(x, y)$. Thus, the $b_i(x, y)$ compensate the spectral overlap of the multiplied filters $a_i(x, y)$ and $a_{i+1}(x, y)$ according to the compensation principle [23][22].

The clipped-eigenvalues operator (dot-responsive cell)

Let $l(x, y)$ denote the image intensity. Eq. 17 for the determinant of the Hessian can then be rewritten as

$$G = \frac{1}{4}(l_{xx} + l_{yy})^2 - \frac{1}{4}(l_{xx} - l_{yy})^2 - l_{xy}^2 = (\nabla^2 l)_2 - \varepsilon^2 \quad (27)$$

The Laplacian and eccentricity ε determine the eigenvalues of the Hessian:

$$d_{1,2} = \nabla^2 l \pm \varepsilon \quad (28)$$

The clipped-eigenvalues operator is defined as

$$C = d_2^+ - d_1^-, \quad (29)$$

where the clipping operation $d^{+/-}$ takes the positive and negative values respectively (one way rectification). Note that C equals the Laplacian for isotropic patches where $\varepsilon = 0$. The operator C has been described and generalised in [23] [2] and [3]; and the relationship to other curvature estimates has been discussed. The multi-scale version of C is obtained by blurring the intensity $l(x, y)$ with a Gaussian kernel.

7. REFERENCES

[1] E H Adelson and J R Bergen. Spatiotemporal energy models for the perception of motion. *Journal of the Optical Society of America*, A2:284–299, 1985.

[2] E Barth, T Caelli, and C Zetzsche. Efficient visual representation and reconstruction from generalized curvature measures. In B. Vemuri, editor, *Geometric Methods in Computer Vision*, volume SPIE 1570, pages 86–95, 1991.

[3] E Barth, T Caelli, and C Zetzsche. Image encoding, labelling and reconstruction from differential geometry. *CVGIP:GRAPHICAL MODELS*, 1993. in press.

[4] E Barth, C Zetzsche, and M Ferraro. Fractal properties of images revealed by a curvature scale-space representation. *Perception*, 21:98, 1992.

[5] J D Farmer. Information dimension and the probabilistic structure of chaos. *Z. Naturforsch.*, 37a:1304–1325, 1982.

[6] I S Gradshteyn and I M Ryzhik. *Table of Integrals, Series and Products*. Academic Press, Orlando,

Florida, 2nd edition, 1980.

[7] J J Koenderink. The structure of images. *Biol. Cybern.*, 50:363–370, 1984.

[8] B B Mandelbrot. *The fractal geometry of nature*. Freeman, New York, 1982.

[9] J M Marstrand. Some fundamental geometrical properties of plane sets of fractional dimensions. *Proc. London Math. Soc.*, 3(4):257–302, 1954.

[10] P Mattila. Integralgeometric properties of capacities. *Transactions of the American Mathematical Society*, 266(2):539–554, August 1981.

[11] C Morrone and D C Burr. Feature detection in human vision: a phase dependent energy model. *Proc. R. Soc. Lond.*, B 235:221–245, 1988.

[12] H O Peitgen and D Saupe. *The Science of Fractal Images*. Springer, New York, Berlin, 1988.

[13] A P Pentland. Fractal-based description of natural scenes. *IEEE Pattern Anal. Machine Intell.*, PAMI-6(6):661–674, 1984.

[14] P Perona and J Malik. Scale-space and edge detection using anisotropic diffusion. *IEEE Pattern Anal. Machine Intell.*, 12(7):629–639, 1990.

[15] B E Rogowitz and R V Voss. Shape perception and low-dimensional fractal boundary contours. In *Human Vision and Electronic Imaging: Models, Methods, and Appplications*, volume SPIE Vol. 1249, pages 389–394, 1990.

[16] L Spillmann and J S Werner, editors. *Visual perception: the neurophysiological foundations*. Academic Press, San Diego, 1990.

[17] H Takayasu. *Fractals in the physical sciences*. Nonlinear Science: Theory and application. Manchester University Press, 1990.

[18] R F Voss. Random fractal forgeries. In R A Earnshaw, editor, *Fundamental Algorithms for Computer Graphics*, pages 805–835. Springer-Verlag, Berlin, 1985.

[19] B Wegman and C Zetzsche. Visual system based polar quantization of local amplitude and local phase of orientation filter outputs. In B Rogowitz, editor, *Human Vision and Electronic Imaging: Models, Methods, and Applications*, volume SPIE 1249, pages 306–317, 1990.

[20] C Zetzsche and E Barth. Fundamental limits of linear filters in the visual processing of two-dimensional signals. *Vision Research*, 30:1111–1117, 1990.

[21] C Zetzsche and E Barth. Image surface predicates and the neural encoding of two-dimensional signal variation. In B. Rogowitz, editor, *Human Vision and Electronic Imaging: Models, Methods, and Applications*, volume SPIE 1249, pages 160–177, 1990.

[22] C Zetzsche and E Barth. Direct detection of flow discontinuities by 3D-curvature operators. *Pattern Recognition Letters*, 12:771–779, 1991.

[23] C Zetzsche and E Barth. Spatio-temporal curvature measures for flow field analysis. In B. Vemuri, editor, *Geometric Methods in Computer Vision*, volume SPIE 1570, pages 337–350, 1991.

[24] C Zetzsche, E Barth, and B Wegmann. The importance of intrinsically two-dimensional image features in biological vision and picture coding. In B Watson, editor, *Visual factors in electronic image communications*. MIT Press, Cambridge, MA, 1993. in press.

[25] C Zetzsche and W Schoeneker. Orientation selective filters lead to entropy reduction in the processing of natural images. *Perception*, 16:229, 1987.